Assessment of Proton Direct Ionization for the Radiation Hardness Assurance of Deep Submicron SRAMs Used in Space Applications

Andrea Coronetti, *Student Member, IEEE*, Rubén Garcìa Alìa, *Member, IEEE*, Jialei Wang, *Graduate Student Member, IEEE*, Maris Tali, Matteo Cecchetto, Carlo Cazzaniga, Arto Javanainen, *Member, IEEE*, Frédéric Saigné, and Paul Leroux, *Senior Member, IEEE*

***Abstract*— Proton direct ionization (PDI) from low-energy protons has been shown to have a potentially significant impact on the accuracy of prediction methods used to calculate the upset rates (URs) of memory devices in space applications for state-of-the-art deep submicron technologies. The general approach nowadays is to consider a safety margin to apply over the UR computed from high-energy proton and heavy-ion experimental data. The data reported here present a challenge to this approach. Different UR prediction methods are used and compared in order to establish the impact of PDI on the total UR. Regardless of the method employed, the findings suggest that PDI can contribute to up to 90% of the total UR, on average, for a general selection of space orbits, with peaks of up to 99%. Such results suggest that an approach based on the characterization of the low-energy portion of the proton spectrum would be more convenient for similar technologies than the application of a general safety margin. Based on data presented here, the previously proposed margin of 5 is exceeded, by large amounts in some cases.**

***Index Terms*— Low-energy protons (LEPs), Monte-Carlo (MC) simulations, prediction methodologies, proton direct ionization (PDI), radiation hardness assurance (RHA), space environment, upset rate (UR).**

Manuscript received December 31, 2020; revised February 15, 2021; accepted February 17, 2021. Date of publication February 22, 2021; date of current version May 20, 2021. This work was supported in part by the European Union's Horizon 2020 Research and Innovation Program through the Marie Sklodowska Curie (MSC) under Grant 721624 and in part by the European Space Agency [ESA/European Space Research and Technology Center (ESTEC)] at the University of Jyväskylä under Contract 4000124504/18/NL/KML/zk.

Andrea Coronetti is with CERN, 1211 Geneva, Switzerland, and also with the Department of Physics, University of Jyväskylä, 40014 Jyväskylä, Finland (e-mail: andrea.coronetti@cern.ch).

Rubén Garcìa Alìa, Maris Tali, and Matteo Cecchetto are with CERN, 1211 Geneva, Switzerland.

Jialei Wang and Paul Leroux are with the Department of Electrical Engineering (ESAT), KU Leuven, 2440 Geel, Belgium.

Carlo Cazzaniga is with the Science and Technology Facilities Council, Didcot OX11 0QX, U.K.

Arto Javanainen is with the Department of Physics, University of Jyväskylä, 40014 Jyväskylä, Finland, and also with the Department of Electrical Engineering and Computer Science, Vanderbilt University, Nashville, TN 37235 USA.

Frédéric Saigné is with the Institute d'Électronique et des Systèmes, Université de Montpellier, 34090 Montpellier, France.

Color versions of one or more figures in this article are available at https://doi.org/10.1109/TNS.2021.3061209.

Digital Object Identifier 10.1109/TNS.2021.3061209

I. Introduction

THE potential impact of direct ionization phenomena arising from singly charged particles, such as protons [1], [2], electrons [3], and muons [4], on the upset rate (UR) of memory devices has been a matter of concern for more than a decade. When it comes to space applications, low-energy protons (LEPs) are one of the main threats challenging the standard UR prediction methodologies based on high-energy proton (HEP) and heavy-ion (HI) single-event upset (SEU) characterizations. Although not specifying how to calculate the UR from LEPs, space standards for single-event effects [5] are starting to mention procedures for SEU characterization under LEP irradiation.

While it is common to refer to HEPs as those protons with energy above 20 MeV, the energy range for LEPs is not clearly defined. One of the reference studies in this subject [6] suggests to account only for protons having energies in the 0–3 MeV range because these are the only energies relevant for direct ionization. Such an observation arose from those previous experimental observations.

An additional source of uncertainty on the total UR may arise from proton elastic scattering, occurring at energies below 20 MeV [7]–[9], which is generally neglected as well.

Both direct ionization and elastic scattering are phenomena that can cause SEUs in deep submicron technologies, regardless of whether they are based on bulk Si or silicon-on-insulator (SOI) processes [10]. Angular dependence was also shown to be an important factor for the triggering of SEU mechanisms. Normal incidence is considered worst case for bulk silicon and 90° tilting worst case for SOI [10].

SEUs from proton direct ionization (PDI) are triggered by the energy directly deposited by protons within the device-sensitive volume (SV). This mechanism becomes more and more remarkable for those protons having an energy near the Bragg peak, that is, those protons that either stop within the SV or that pass through it while depositing most of their energy. These are protons that enter the SV with energies on the order of 50 keV.

In terms of radiation hardness assurance (RHA) for space missions, several approaches have been proposed in the past

years for PDI UR predictions starting from ground test data [6], [10]–[13]. One of the main studies [6] proposes the use of a degraded HEP beam as an enabler for LEP SEU ground testing. In this case, the main advantage is the possibility to exploit the energetic spread introduced by the degraders in the beamline to irradiate the device with a spectra replicating that found in a typical Earth space mission in the 0–3 MeV energy range.

The main conclusion of the study was that for static random access memories (SRAM) operated down to 10% undervoltage, the PDI contribution to the total UR could be counted by applying a conservative margin of 5 to the UR calculated from the conventional HEP and HI SEU cross sections determined through ground testing [10].

The present work explores very strong PDI enhancements observed in the SEU cross sections of a few SRAMs that can break the previous assumptions about the severity of PDI for space missions RHA. When considering the two commercial devices in the accelerator context [14], it was found that UR enhancements due to PDI up to a factor of 5 were expected. This despite the minor contribution of LEPs to the overall accelerator radiative environment (largely neutron-dominated) if compared to the larger abundance of LEPs in the space environment. Thus, the objective is to determine whether the standard RHA approaches for PDI are challenged by this specific set of devices and by how much the previous safety margins might be violated.

This article is structured as follows. The experimental investigation performed for this work is briefly introduced. The experimental data are fed into models to be used in Monte-Carlo (MC) simulation tools. These are used, along with other prediction tools to estimate the UR of the characterized devices for a few selected space orbits in order to evaluate the impact of PDI UR in typical space missions.

II. Experimental Investigation

One of the three characterized devices is a custom-developed SRAM designed by one of the authors of this article and the other two are commercial SRAMs. The custom-developed SRAM will henceforth be referred as RADSAGA 65-nm SRAM. As the name suggests, it is based on a 65-nm technology and it was manufactured according to the standard commercial Taiwan Semiconductor Manufacturing Company (TSMC) process. The only difference is that the cell size is three times larger than that of the standard. One of the commercially available SRAMs, reference CY62167GE30-45ZXI (henceforth called Cypress SRAM), is also based on this technology. The other commercial SRAM, reference IS61WV204816BLL-10TLI (henceforth called Integrated Silicon Solutions Inc. (ISSI) SRAM), is based on a 40-nm technology. The main features of these memories are summarized in Table I.

Note that the RADSAGA 65-nm SRAM [15] has a tunable core voltage that can be used to vary the sensitivity of the memory chip, spanning in the 0.3–1.2 V range. For the scope of this article, the presented data and the main focus will be devoted to a core voltage of 0.3 V. The data presented for the commercial SRAMs all refer to their nominal core voltages of 1.1 V. Note that the Cypress SRAM has an internal error-correction code (ECC), which has been disabled for the purposes of this study.

TABLE I
SRAMs Under Consideration in This Work

Name	Technology (nm)	Size (bits)	Core Voltage (V)
RADSAGA	65	32k	0.3
ISSI	40	32M	1.1
Cypress	65	16M	1.1

TABLE II
Main Characteristics of the HIs Used to Characterize the SEU Cross Sections

Ion	Energy (MeV)	LET (MeV/(mg/cm^2))	Range (mm)
C	1080	0.22	11.78
C	720	0.31	5.73
C	360	0.52	1.67
Ar	1050	5.2	0.55
Ar	548	8.1	0.20
Xe	2700	43.5	0.22

The SRAMs have been tested with several beams [16] and most of the experimental details are reported in that article. All the SRAMs have been irradiated through the back-end-of-line (BEOL). This was shown to have an impact for SOI SRAMs [17] with respect to irradiation from the substrate. For the presented bulk SRAMs, however, such configuration could not be achieved.

For the purpose of this work, data referring to LEP, HEP, and HI irradiations are reported. Concerning LEPs, the core of the experimental work was completed at the Centro Nacional de Aceleradores (CNA) [18]. There, the SRAMs have been irradiated with mono-energetic proton beams in the 0.5–5 MeV energy range. LEP data for the ISSI SRAM were collected at the Radiation Effects Facility (RADEF) [19], [20] at the University of Jyväskylä. HEP testing was accomplished at the Kernfysisch Versneller Instituut (KVI) [21] for the ISSI and Cypress SRAMs and at the Paul Scherrer Institute (PSI) [22] for the RADSAGA 65-nm SRAM. HI testing was performed at KVI for all the SRAMs. Table II reports the HI characteristics in terms of species, energy, linear energy transfer (LET), and range. Only the LEP testing at CNA and RADEF were performed in vacuum. All the data have been obtained at normal incidence and room temperature. Different from other experiments and measurement techniques [23], [24], mono-energetic LEP data have not been obtained by beam degradation.

Error bars for all experimental data are calculated at 95% confidence level, assuming a fluence uncertainty of 10% and based on the actual number of events. If not visible in the plots, they are smaller than the markers.

The experimental proton cross sections as a function of energy for the RADSAGA 65-nm SRAM are depicted in Fig. 1. The peak direct ionization cross section was found for 900 keV and it reaches up to 4×10^{-9} cm^2/bit. The cross section is still higher than 10^{-12} cm^2/bit at 5 MeV. The HEP cross section lowers down to 1.5×10^{-13} cm^2/bit

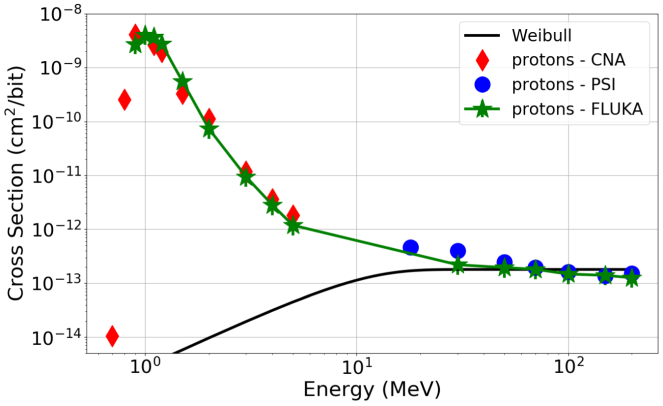

Fig. 1. Low and HEP experimental cross sections as a function of proton energy for the RADSAGA 65-nm SRAM when tuned at 0.3 V. The HEP data are fit with a Weibull with the following parameters: $\sigma_{sat} = 1.8 \times 10^{-13}$ cm^2/bit, $E_0 = 0$ MeV, $W = 10$ MeV, $s = 1.8$. The data are compared with the FLUKA simulated cross sections.

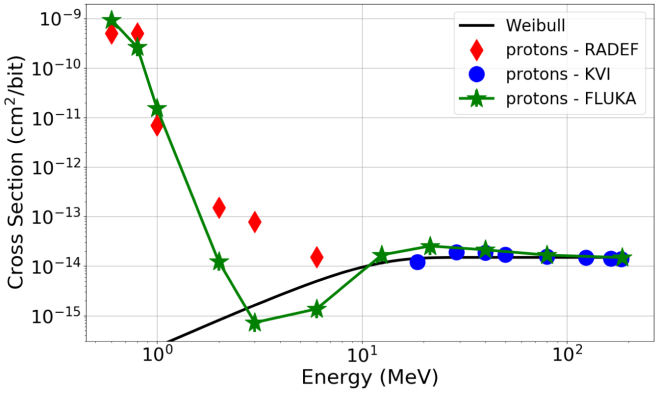

Fig. 2. Low and HEP experimental cross sections as a function of proton energy for the ISSI SRAM. The HEP data are fit with a Weibull with the following parameters: $\sigma_{sat} = 1.5 \times 10^{-14}$ cm^2/bit, $E_0 = 10$ MeV, $W = 0$ MeV, $s = 1.8$. The data are compared with the FLUKA simulated cross sections.

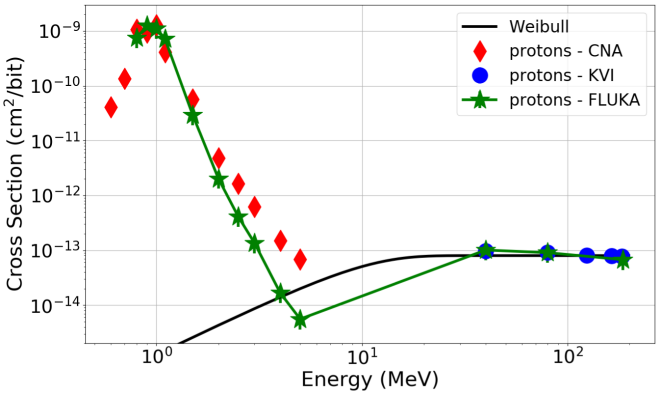

Fig. 3. Low and HEP experimental cross sections as a function of proton energy for the Cypress SRAM. The HEP data are fit with a Weibull with the following parameters: $\sigma_{sat} = 8 \times 10^{-14}$ cm^2/bit, $E_0 = 10$ MeV, $W = 0$ MeV, $s = 1.8$. The data are compared with the FLUKA simulated cross sections.

at 200 MeV. It is seen to grow from below 100 MeV to reach up to 4.7×10^{-13} cm^2/bit at 18 MeV. This may indicate a potential influence of direct ionization at energies around 20 MeV. For the Weibull fit, the saturation cross section is taken to be 1.8×10^{-13} cm^2/bit to better account for this enhancement below 100 MeV. Overall, the peak PDI cross section is about 2.2×10^4 times the HEP saturation cross section used for the Weibull fit.

The experimental proton cross sections as a function of energy for the ISSI SRAM are depicted in Fig. 2. The peak direct ionization cross section was observed at 600–800 keV, probably indicating a thinner BEOL than the previous SRAM. The fact that the LEP cross section is almost constant for an interval of energies (600–800 keV) more strongly points out the reaching of the physical limit imposed by the SV size. The peak cross section is 5×10^{-10} cm^2/bit. The HEP saturation cross section is 1.5×10^{-14} cm^2/bit, resulting in a ratio between the peak PDI and high-energy saturation cross sections of 3.3×10^4.

The indicated ratios are among the highest that could be found in the literature. In one case [25], ratios up to a factor of 10^5–10^6 were observed. However, different from these data, the peaks were quite steep and narrow, indicating a higher critical charge than for the devices here considered.

The experimental proton cross sections as a function of energy for the Cypress SRAM are depicted in Fig. 3. The peak direct ionization cross section is seen to occur between 800 keV and 1 MeV, stretching up to 1.2×10^{-9} cm^2/bit. The HEP saturation cross section is 8×10^{-14} cm^2/bit. As a result, the ratio between the peak PDI and high-energy saturation cross sections is 1.5×10^4.

Fig. 4 presents the same PDI data for the RADSAGA 65-nm SRAM as a function of LET compared to cross sections obtained with long range ions. Other than the data points at high LET, which define the HI saturation cross section, the main purpose of the figure is to compare the cross sections of LEPs with those of long-range high-energy light ions (carbon in the 30–90 MeV/u energy range).

In the figure, ion data points have been placed at an LET corresponding to that before the BEOL. It is assumed that, given their longer range, the ions will reach the SV while losing a negligible amount of energy in the BEOL. On the contrary, LEPs have a shorter range that may bring them to stop either inside the SV or in its vicinity. Thus, LEP data points have not been placed at the tabulated LET [26] for that primary energy before the BEOL. A more realistic LET has been estimated based on the interaction with the BEOL. While the latter cannot be known for the commercial memories, the experimental cross section helped deducing their SiO_2 equivalent BEOL thicknesses. On the other hand, for the RADSAGA 65-nm SRAM, it is known from manufacturing documentation that the BEOL would be equivalent to a layer of SiO_2 12-μm thick.

Whether known or deduced from the data, this equivalent thickness was used to calculate the energy lost by the primary protons while passing through the BEOL by means of the stopping and range of ions in matter (SRIM) software [27]. Once this was known, SRIM was again used to determine the range in silicon of a proton having the residual kinetic energy and calculate an LET based on this residual kinetic energy

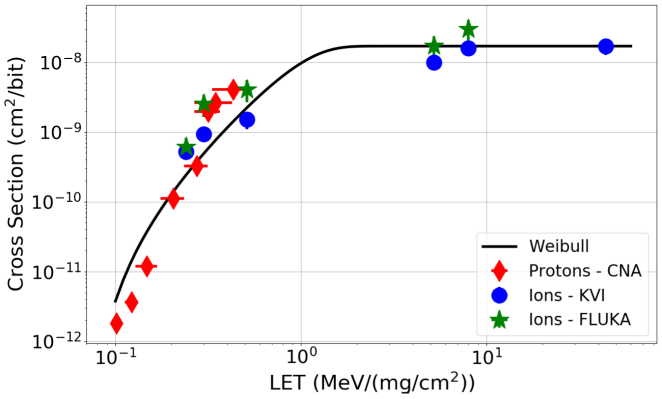

Fig. 4. LEP and HI cross sections as a function of LET for the RADSAGA 65-nm SRAM when tuned at 0.3 V. Weibull parameters: $\sigma_{sat} = 1.7 \times 10^{-8}$ cm^2/bit, LET$_0$ = 0.07 MeV/(mg/cm^2), W = 1 MeV/(mg/cm^2), $s = 2.4$. The data are compared with the FLUKA simulated cross sections.

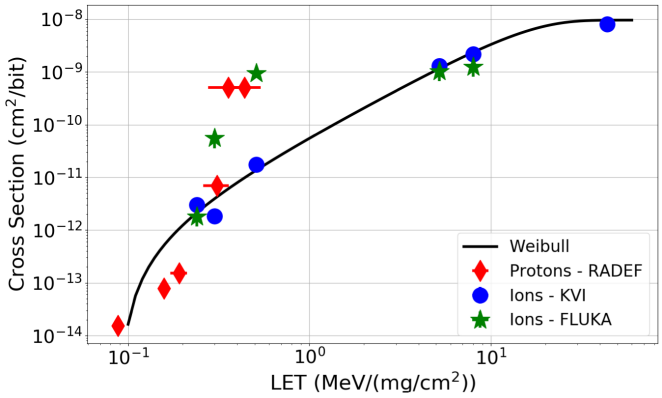

Fig. 5. LEP and HI cross sections as a function of LET for the ISSI SRAM. Weibull parameters: $\sigma_{sat} = 9.56 \times 10^{-9}$ cm^2/bit, LET$_0$ = 0.09 MeV/(mg/cm^2), W = 16 MeV/(mg/cm^2), and $s = 1.8$. The data are compared with the FLUKA simulated cross sections.

and the range. This LET is exclusively used to show the LEP points in the plots.

Note that this method introduces an approximation, since it considers that all the protons transiting through the BEOL will experience the same identical energy loss. Fluktuierende Kaskade (FLUKA) 4.0 [28], [29] was used to simulate mono-energetic 900-keV protons traveling through the BEOL oxide. Due to straggling, the resulting spectra after the BEOL and at the entry of the SV were found to be continuous between 0 and 200 keV. This was also observed in [30]. At the same time, the residual kinetic energy obtained from SRIM for this case was about 290 keV. Considering the energy straggling, using a single LET derived from a single proton energy may result in an underestimation of the LET of less than 0.1 MeV/(mg/cm^2), which will not alter the general picture.

Coming back to Fig. 4, it is clear that the peak PDI cross sections are not fully reproduced by long-range light ions, as was found before [31]. In this case, the peak PDI cross section can be three times higher than the respective carbon cross section at a similar LET.

Fig. 5 shows the LEP and HI cross sections as a function of LET for the ISSI SRAM. The same procedure, as for the

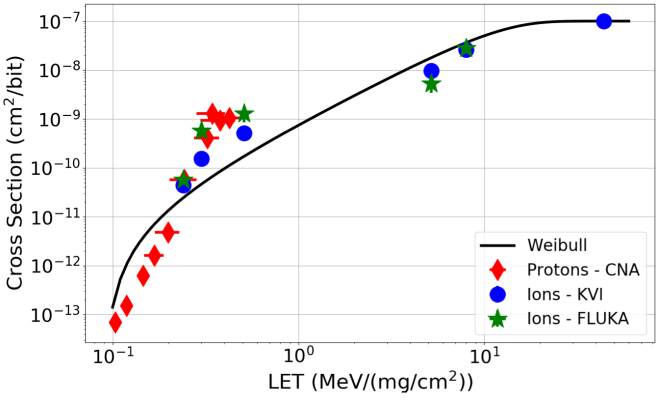

Fig. 6. LEP and HI cross sections as a function of LET for the Cypress SRAM. Weibull parameters: $\sigma_{sat} = 1 \times 10^{-7}$ cm^2/bit, LET$_0$ = 0.09 MeV/(mg/cm^2), W = 12 MeV/(mg/cm^2), and $s = 1.9$. The data are compared with the FLUKA simulated cross sections.

previous case, was implemented for the LEP LET determination, this time with a BEOL as thick as 6 μm. The PDI peak is seen to exceed the carbon cross sections for similar LET by even a factor of 50. Indeed, the peak PDI cross sections are even closer to the argon ion cross sections obtained with LETs above 5 MeV/(mg/cm^2) than to the carbon ion cross sections.

Fig. 6 depicts the LEP and HI cross sections as a function of LET for the Cypress SRAM. The LETs for LEPs were calculated assuming a BEOL 10-μm thick. This was chosen because the PDI peak cross section is maximum between 0.8 and 1 MeV and it starts fading only below 800 keV. Hence, at an energy lower than where the fading is observed for the RADSAGA 65-nm SRAM. The situation is similar to the RADSAGA 65-nm SRAM, with a maximum difference among peak PDI and carbon ion cross sections of a factor of 3.

The reason for the observed experimental behaviors is not fully clear, but it is not caused by the presence of multiple-bit upsets (MBUs, occurring in the same word), while nothing can be said about multiple-cell upsets (MCUs, occurring in physically adjacent cells) given that the physical mapping of the memories is not available. It may be a topic of future investigations. The presented HI LET Weibull functions are derived to follow the HI data at both low and high LET and will be later used to calculate the HI contributions to the total UR.

Carbon and argon ion interactions were also simulated with FLUKA and are reported in the figures. For all the models, the FLUKA-simulated cross sections for carbon (low LET) tend to follow the LEP experimental data rather than the carbon experimental data at similar LET. This is particularly evident for the ISSI SRAM (Fig. 5). On the other hand, the agreement between argon experimental data and simulated data is within a factor of 2 for all the models.

III. Modeling of the SVs

SV models are proposed for the memory cells of the three SRAMs. They will be used as input in the MC simulations used to determine the UR of the SRAMs in the space environment.

TABLE III

NESTED RPP DATA OF THE SVS OF EACH SRAM ALONG WITH THE COLLECTION EFFICIENCY (ALPHA), BEOL THICKNESS, AND CRITICAL CHARGE

RADSAGA 65 nm SRAM		
BEOL 12 μm, Q_{crit} = 0.55 fC		
SV side (nm)	**SV thickness (nm)**	**alpha**
638	250	1
996	250	0.077
1304	250	0.050
ISSI SRAM		
BEOL 6 μm, Q_{crit} = 0.96 fC		
SV side (nm)	**SV thickness (nm)**	**alpha**
310	310	1
Cypress SRAM		
BEOL 10 μm, Q_{crit} = 0.86 fC		
SV side (nm)	**SV thickness (nm)**	**alpha**
360	360	1
984	360	0.057
1612	360	0.037
3160	360	0.007

All the SRAM models here considered are based on rectangular parallelepiped (RPP) that are built based on the experimental data. LEP data are very useful when building such models since they can give direct indications of the SV size, that is, the direct ionization cross section tends to be equal to the SV surface normal to the beam. In addition, the lowering of the cross section at energies below the PDI peak can give indications about the BEOL thickness. Finally, the slope of the cross section curve from the PDI peak toward higher energies can give indications about the SV thickness and the critical charge Q_{crit} [14].

Even when these LEP data are correctly fit, often a single RPP can be representative of the LEP cross section, but it can underestimate the HEP cross section. Given that the models will be used for the estimations of the UR due to LEPs and HEPs, as well as HIs, it is crucial to build models that could reproduce in the best possible way also the high-energy part of the proton cross section. A nested RPP technique [11], [32] based on HI data can be used to better fit the HEP cross section while not affecting the low-energy part.

The nested RPP technique was used for the RADSAGA 65-nm and Cypress SRAMs. On the other hand, a single RPP was found to be suitable for the ISSI SRAM since it fairly reproduces both the LEP and HEP responses. The data of the RPP models for all the SRAMs are reported in Table III. The BEOL are assumed to be made with SiO_2 for all the cases.

For the nested RPPs, the external volume sides are obtained directly by a few high-LET HI ($>$5 MeV/(mg/cm^2)) cross section data points. The collection efficiency (alpha) is obtained by making the ratio between the LET of the PDI peak data point and the LET of that HI. For the RADSAGA 65-nm SRAM, the reference proton LET is 0.4 MeV/(mg/cm^2), whereas for the Cypress SRAM, this is 0.3 MeV/(mg/cm^2). The thickness is kept constant [33] and equal to that of the innermost SV (targeted to reproduce the PDI enhancement).

The RADSAGA 65-nm SRAM has the largest SV side (640 nm) for the innermost volume. At the same time, this is the only model for which the SV thickness (250 nm) did not coincide with the SV side. The reason is the matching of the proton cross section at energies of 1–5 MeV. Using a larger thickness would lead the simulated cross section to fall down much quicker with increasing energy. The critical charge is also the lowest (0.55 fC), given the lower core voltage. For the outermost volumes, only the argon ion data are retained, since the xenon data point has the same cross section as the argon ion with the highest LET.

TABLE IV

COMPARISON OF THE ENERGY CONVOLUTION OF THE EXPERIMENTAL AND RPP MODEL PROTON RESPONSES FOR LOW- (0–3 MeV), INTERMEDIATE- (3–20 MeV), AND HIGH-ENERGY ($>$20 MeV) REGIONS FOR THE THREE SRAMS WITH THE ISS ENVIRONMENT AND 100 MILS OF ALUMINUM SHIELDING. DATA ARE REPORTED IN SEU/bit/day

Data	**0-3 MeV**	**3-20 MeV**	**$>$ 20 MeV**	**Total**
RADSAGA 65 nm SRAM				
Exp	8.00 x 10^{-6}	4.37 x 10^{-7}	5.90 x 10^{-7}	9.03 x 10^{-6}
RPP	9.06 x 10^{-6}	2.94 x 10^{-7}	4.59 x 10^{-7}	9.81 x 10^{-6}
ISSI SRAM				
Exp	6.22 x 10^{-7}	5.38 x 10^{-9}	4.14 x 10^{-8}	6.69 x 10^{-7}
RPP	6.76 x 10^{-7}	3.80 x 10^{-9}	4.53 x 10^{-8}	7.25 x 10^{-7}
Cypress SRAM				
Exp	1.89 x 10^{-6}	2.34 x 10^{-8}	2.22 x 10^{-7}	2.14 x 10^{-6}
RPP	2.11 x 10^{-6}	7.64 x 10^{-9}	2.08 x 10^{-7}	2.33 x 10^{-6}

The ISSI SRAM has the lowest PDI peak cross section, hence the lowest RPP side (310 nm). It also has the thinner BEOL (6 μm) since the memory was experimentally observed to be sensitive down to just 600 keV. Finally, it also relies on the highest critical charge (0.96 fC), which, in spite of the smaller technology, is likely due to differences in the manufacturing processes among companies.

For the innermost volume, the Cypress SRAM model has the SV side and thickness of 360 nm. The critical charge is 0.86 fC. To complete the model, three larger volumes are added based on the argon and xenon cross sections. In this case, the HI saturation cross section is much larger than that of the RADSAGA 65-nm SRAM, resulting in volumes with sides as large as 3 μm.

FLUKA MC simulations were performed for all the models and for several mono-energetic proton cases to assess the consistency of the model with respect to the experimental data. The uncertainty on the calculated cross sections varies with each energy. On average, an uncertainty of $\pm 35\%$ can be taken for all the data points and models based on the energy deposition distributions. Other uncertainties may be present on the parameters chosen for the SV such as BEOL thickness, critical charge, SV size, and thickness.

Figs. 1–3 present the comparison among the mono-energetic experimental and simulated cross sections for the RADSAGA 65-nm SRAM, ISSI SRAM, and Cypress SRAM, respectively.

For the RADSAGA 65-nm SRAM, the consistency is verified at low (0–3 MeV), intermediate (3–20 MeV), and high energy ($>$20 MeV). For the ISSI and Cypress SRAMs, the agreement between the models and the experiments is good for LEPs and HEPs. For the intermediate-energy region, the agreements are less optimal. However, this region is not an important contributor when it comes to the proton UR since it contributes less than 1%, at least for these two SRAMs.

As a further verification of the validity of the proposed RPP models to describe the proton cross section response over different sets of energies, a first UR calculation was performed. cosmic-ray environment and effects models (CREME) 96 [34] was used to determine the trapped proton flux for the International Space Station (ISS) orbit. The flux was transported by means of the online tool through 100 mils of aluminum. The data were then divided into the three energy regions described before. Both the experimental data and the RPP model data were convolved along with the proton fluxes in the three energy regions. Both data sets are determined for normal incidence only, for both the data and the radiation field. For this simple calculation, the angular response is not considered because no such experimental data were collected and a fair comparison would not be possible.

Table IV reports the comparison of all three devices and for each energy region. The agreement for each region is quite satisfactory. The largest discrepancies are seen for the ISSI and Cypress SRAMs for intermediate-energy protons. However, given that, for these memories, this region is expected to contribute 1% or less to the total UR, the related inaccuracy can be assumed to be negligible. Globally, the total URs from these models are about 10% higher than their experimental counterparts.

IV. UR Prediction Methods

UR prediction methods based on the measurements of HEP and HI cross sections are nowadays well standardized, for example, the Weibull [35] method, among others. Existing methods on HEPs and HIs are all based on the assumptions made from the typical test results that cross section curves are null below the energy/LET threshold and tend to reach a saturation cross section at high energy/LET while maintaining a monotonic dependence with energy/LET.

PDI, however, introduces the problem that the cross section is no longer monotonic with energy. Hence, the established prediction methods can hardly help out in predicting the UR from LEPs. In principle, some of these methods can be mimicked in some other way, because they are basically convolutions of a cross section function defined as a function of energy/LET with an environmental particle spectrum, similarly defined as a function of energy/LET.

The LEP experimental mono-energetic cross sections can, for instance, be convolved with the environmental flux without a need to define a function that would describe the whole cross section curve as a function of energy, that is, by performing linear interpolation for intermediate points. This is supposed to provide a more accurate estimation than that obtained by multiplying the cross section peak for the proton flux in the relevant energy range, as proposed in [36].

Still, among the problems introduced by energy convolution, there is the assumption that the proton will reach the SV with normal incidence, which is not the case since the space environmental proton fluxes are isotropic. For instance, when folding the cross sections presented in Fig. 1, all protons within the environment having an energy below 700 keV will not contribute to the response. However, when considering an isotropic spectrum, there will always be protons arriving at the SV with an energy in the 0-700-keV range, which, in principle, are associated with a cross section similar with that of the PDI peak. Such a method, based on the energy and range of protons arriving at the SV, was also proposed in the past [37].

Another possibility would be to treat the LEPs in a similar fashion as HIs and to perform an LET convolution. However, in this case, determining the LET of the protons used during the experiments can, as was shown before, be complicated and the uncertainty introduced by the straggling may lead to much higher inaccuracy than for the determination of the actual proton energy.

A promising method, proposed by Dodds [6], to calculate the UR from PDI consists of measuring the cross section of a degraded high-energy beam containing a known spectrum of LEPs. The method also requires performing measurements at various angles of incidence to cover the effects related to the isotropic nature of the space spectra. The PDI UR is then compared to those attained through the Weibull method for HEPs and HIs. However, when data from such an experiment are not available, approximate methods may be introduced based on the observed mono-energetic proton cross sections in order to retrieve the UR.

Finally, MC simulations can also be considered for UR predictions. The earlier introduced RPP models of the SV can be used to extract the cross sections derived from the environmental proton and HI spectra. The advantage of MC simulations is that the models used are assumed to be a valid representation of the device response regardless of the particle or energy. In addition, they may also provide further indications about potential variations introduced by varying the parameters in the chosen models. Note that the MC simulations are run with isotropic spectra as input, hence accounting for the angular response of the modeled component. A certain degree of uncertainty, which is not so easy to quantify, is present, anyhow. This is due to the lack of experimental data at different angles of incidence. That is, the angular dependence here considered is that emerging as a result of the modeling at normal incidence, but no verification with respect to experimental data was possible.

For this first assessment, the data refer to a single orbit and a single shielding configuration. The environment under consideration is that of the ISS for solar minimum conditions. Both proton and HI fluxes are transported through 100 mils of aluminum with the CREME/universal heavy ion propagation code (UPROP) online tool. The fluxes are then used to perform energy convolution calculations (applicable only to protons), the Weibull fit calculations (applicable only to HEPs and HIs), FLUKA MC simulations (applicable to every particle and energy), and an approximated Dodds' method (applicable only to LEPs).

For the heavy-ion Weibull methods, the Weibull curves presented in Figs. 4–6 were used. For the HEPs, the same identical Weibull functions were used for the three devices, but with a different saturation cross section ($E_{\text{th}} = 0$ MeV, $W = 10$ MeV, $s = 1.8$). The saturation cross sections were 1.8×10^{-13}, 1.5×10^{-14}, and 8×10^{-13} cm^2/bit for the RADSAGA 65-nm ISSI and Cypress SRAMs, respectively (Figs. 1–3).

TABLE V

COMPARISON OF UR PREDICTION METHODS FOR LOW AND HEPS AND HIS FOR THE THREE SRAMS AT 0.3 V FOR THE LISTED METHODS. THE ISS ENVIRONMENT IS USED FOR ALL METHODS (500 km, 51.6°, SOLAR MIN, 100 MILS ALUMINUM). THE UR UNITS ARE SEU/bit/day

RADSAGA 65 nm SRAM			
Method	**High-E protons**	**Low-E protons**	**Heavy ions**
Energy convolution	5.42 x 10^{-7}	8.49 x 10^{-6}	X
Weibull	4.57 x 10^{-7}	X	2.65 x 10^{-7}
Monte-Carlo	3.04 x 10^{-7}	1.47 x 10^{-5}	4.07 x 10^{-7}
Approx. Dodds'	4.57 x 10^{-7}	1.43 x 10^{-5}	2.65 x 10^{-7}
ISSI SRAM			
Method	**High-E protons**	**Low-E protons**	**Heavy ions**
Energy convolution	4.06 x 10^{-8}	6.27 x 10^{-7}	X
Weibull	3.81 x 10^{-8}	X	3.90 x 10^{-9}
Monte-Carlo	2.33 x 10^{-8}	5.76 x 10^{-7}	5.34 x 10^{-8}
Approx. Dodds'	3.81 x 10^{-8}	1.20 x 10^{-6}	3.90 x 10^{-9}
Cypress SRAM			
Method	**High-E protons**	**Low-E protons**	**Heavy ions**
Energy convolution	2.25 x 10^{-7}	1.92 x 10^{-6}	X
Weibull	2.03 x 10^{-7}	X	4.02 x 10^{-8}
Monte-Carlo	1.58 x 10^{-7}	1.88 x 10^{-6}	1.10 x 10^{-7}
Approx. Dodds'	2.03 x 10^{-7}	3.41 x 10^{-6}	4.02 x 10^{-8}

The idea behind the approximated Dodds' method is to retrieve a rough estimate of the cross section that would have been measured for the devices presented in this work if experimental measurements in a high-energy degraded beam were performed. Note that the Dodds' method can be used to calculate the LEP contribution to the UR, whereas for the HEP and HI contributions, the method also relies on the Weibull fits.

The approximated Dodds' method consists in the convolution of the experimental LEP cross section with the spectrum experimentally measured at Tri-University Meson Facility (TRIUMF) [6] when degrading the 70-MeV proton beam to an average energy of 6 MeV. Once this cross section is estimated, the approximated method follows the same steps as the original Dodds' method.

Table V presents the UR calculated for the three contributors: LEPs, HEPs, and HIs with the various methods. Note that in this case all protons in the environment below 20 MeV are considered as LEPs, as they are typically irrelevant in the traditional methods based on HEP and HI characterizations only.

For all three devices, the energy convolution, Weibull, and MC methods deliver very similar HEP URs, always within less than a factor of 2 difference. For HIs, the Weibull and the MC methods are quite in disagreement for the ISSI SRAM, with even one order of magnitude lower UR delivered by the Weibull fit. For the other two SRAMs, the differences are much smaller, within a factor of 1.5 for the RADSAGA 65-nm SRAM and less than a factor of 3 for the Cypress SRAM. The larger HI UR arising from MC simulations is due to the fact that the RPP models of the SVs are built so that they follow the experimental LEP cross sections at low LET rather than the light ion cross sections. As was shown earlier, the difference is not negligible, in particular, for the ISSI SRAM, for which the discrepancy between different HI UR estimation methods is the highest.

Concerning the comparison among LEP UR prediction methods, the results are not always consistent among devices. For the RADSAGA 65-nm SRAM, the energy convolution delivers a UR which is about half that of the MC simulations and the approximated Dodds' method, which, in turn, are very similar. This effect may be related to the isotropic nature of the environment, which is neglected in the energy convolution method. However, although this is indeed always the case for all the memories when comparing energy convolution and approximated Dodds' method, for the ISSI and Cypress SRAMs, the MC LEP UR is similar to that obtained through energy convolution.

Since the combined Weibull/Dodds' method and the MC simulations provide data for all three contributors to the total UR, these two approaches are followed to perform the following RHA assessments. One of the main differences between the two methods is that the approximated Dodds' method considers only protons with energy below 3 MeV, whereas the MC simulations consider the full proton spectra below 20 MeV.

V. PDI IMPACT ON THE TOTAL UR

Generally, the UR of a digital device in any space orbit is defined by two main contributions, that is, direct HI ionization and proton indirect ionization. PDI can be considered as a separate contributor since the proton-induced SEUs are, in this case, triggered in a similar fashion as those from HIs. In order to evaluate the impact of PDI on the total UR, let us define a parameter D as

$$D = \frac{\mathrm{UR_{HI}} + \mathrm{UR_{HEP}} + \mathrm{UR_{LEP}}}{\mathrm{UR_{HI}} + \mathrm{UR_{HEP}}}. \tag{1}$$

The D factor will define the relative contribution of PDI to the UR with respect to the UR estimated when PDI is neglected. It can also be seen as a safety margin to apply to the estimated UR when LEP data are not available.

The analysis is made considering the three devices presented in this article, four different space radiation environments, and two different shielding configurations. All the environments are calculated through the CREME96 online tools. The ISS environment (I1 and I5) is calculated at 500-km altitude, 51.6° inclination, solar minimum, quiet conditions; the low-Earth orbit (LEO) environment (L1 and L5) at 1400-km altitude, 52°, solar minimum, quiet conditions; the geostationary orbit (GEO) environment is calculated for both quiet (GQ1 and GQ5) and stormy solar conditions (GW1 and GW5, worst day). The shielding configurations are with 100 and 500 mils of aluminum.

For the RADSAGA 65-nm SRAM, the contributions to the UR (both in absolute and percentage terms) are reported in Table VI for both the MC simulations and for the approximated Dodds' method. PDI effects are found to be negligible only for the GEO quiet conditions, for which both methods, regardless of the shielding, yield a PDI UR in the order of 1%. For all other radiation environments, the PDI contribution to the UR is never below 85%. The most affected orbits are the LEO and GEO in stormy conditions and the situation does not change much when a thicker shielding is considered. Generally, the two methods yield very similar results for

TABLE VI

UR OF THE **RADSAGA 65** -nm **SRAM** FROM PROTON INDIRECT AND DIRECT IONIZATION AND HIS (WITH PERCENTAGE CONTRIBUTIONS TO THE TOTAL UR IN BRACKETS) FOR EIGHT COMBINATIONS OF ORBITS AND SHIELDING CONFIGURATIONS. UR IN SEU/bit/day

Monte-Carlo			
Env.	**UR**$_{HEP}$ **(%)**	**UR**$_{LEP}$ **(%)**	**UR**$_{HI}$ **(%)**
I1	3.04 x 10^{-7} (2%)	1.47 x 10^{-5} (96%)	2.65 x 10^{-7} (2%)
I5	2.41 x 10^{-7} (6%)	3.72 x 10^{-6} (89%)	2.39 x 10^{-7} (6%)
L1	2.38 x 10^{-5} (2%)	1.03 x 10^{-3} (98%)	3.98 x 10^{-7} (0%)
L5	7.72 x 10^{-6} (4%)	2.07 x 10^{-4} (96%)	3.59 x 10^{-7} (0%)
GQ1	3.94 x 10^{-8} (2%)	1.89 x 10^{-8} (1%)	1.84 x 10^{-6} (97%)
GQ5	4.09 x 10^{-8} (3%)	1.79 x 10^{-8} (1%)	1.46 x 10^{-6} (96%)
GW1	3.92 x 10^{-4} (0%)	1.44 x 10^{-1} (96%)	6.04 x 10^{-3} (4%)
GW5	5.98 x 10^{-5} (1%)	5.04 x 10^{-3} (98%)	6.27 x 10^{-5} (1%)
Approximated Dodds' method			
Env.	**UR**$_{HEP}$ **(%)**	**UR**$_{LEP}$ **(%)**	**UR**$_{HI}$ **(%)**
I1	4.57 x 10^{-7} (3%)	1.43 x 10^{-5} (95%)	2.65 x 10^{-7} (2%)
I5	3.32 x 10^{-7} (9%)	3.32 x 10^{-6} (85%)	2.39 x 10^{-7} (6%)
L1	2.29 x 10^{-5} (2%)	9.79 x 10^{-4} (98%)	3.98 x 10^{-7} (0%)
L5	1.64 x 10^{-5} (9%)	1.76 x 10^{-4} (91%)	3.59 x 10^{-7} (0%)
GQ1	5.96 x 10^{-8} (3%)	1.48 x 10^{-8} (1%)	1.84 x 10^{-6} (96%)
GQ5	5.77 x 10^{-8} (4%)	1.72 x 10^{-8} (1%)	1.46 x 10^{-6} (95%)
GW1	3.89 x 10^{-4} (0%)	1.36 x 10^{-1} (96%)	6.04 x 10^{-3} (4%)
GW5	9.65 x 10^{-5} (2%)	4.94 x 10^{-3} (97%)	6.27 x 10^{-5} (1%)

TABLE VII

UR OF THE **ISSI SRAM** FROM PROTON INDIRECT AND DIRECT IONIZATION AND HIS (WITH PERCENTAGE CONTRIBUTIONS TO THE TOTAL UR IN BRACKETS) FOR EIGHT COMBINATIONS OF ORBITS AND SHIELDING CONFIGURATIONS. UR IN SEU/bit/day

Monte-Carlo			
Env.	**UR**$_{HEP}$ **(%)**	**UR**$_{LEP}$ **(%)**	**UR**$_{HI}$ **(%)**
I1	2.33 x 10^{-8} (4%)	5.76 x 10^{-7} (96%)	3.90 x 10^{-9} (1%))
I5	3.94 x 10^{-8} (32%)	8.13 x 10^{-8} (65%)	3.45 x 10^{-9} (3%)
L1	2.47 x 10^{-6} (6%)	4.00 x 10^{-5} (94%)	5.77 x 10^{-9} (0%)
L5	8.27 x 10^{-7} (14%)	5.54 x 10^{-6} (86%)	5.14 x 10^{-9} (0%)
GQ1	6.01 x 10^{-9} (14%)	2.50 x 10^{-9} (6%)	3.50 x 10^{-8} (80%)
GQ5	2.40 x 10^{-9} (8%)	3.44 x 10^{-9} (11%)	2.49 x 10^{-8} (81%)
GW1	8.81 x 10^{-5} (2%)	5.04 x 10^{-3} (97%)	4.46 x 10^{-5} (1%)
GW5	8.62 x 10^{-6} (4%)	4.14 x 10^{-4} (96%)	4.35 x 10^{-7} (0%)
Approximated Dodds' method			
Env.	**UR**$_{HEP}$ **(%)**	**UR**$_{LEP}$ **(%)**	**UR**$_{HI}$ **(%)**
I1	3.81 x 10^{-8} (3%)	1.20 x 10^{-6} (97%)	3.90 x 10^{-9} (0%)
I5	2.77 x 10^{-8} (8%)	3.04 x 10^{-7} (91%)	3.45 x 10^{-9} (1%)
L1	1.91 x 10^{-6} (6%)	8.20 x 10^{-5} (94%)	5.77 x 10^{-9} (0%)
L5	1.37 x 10^{-6} (8%)	1.48 x 10^{-5} (92%)	5.14 x 10^{-9} (0%)
GQ1	5.44 x 10^{-9} (13%)	1.24 x 10^{-9} (3%)	3.50 x 10^{-8} (84%)
GQ5	5.26 x 10^{-9} (17%)	1.44 x 10^{-9} (5%)	2.49 x 10^{-8} (78%)
GW1	3.24 x 10^{-5} (1%)	1.14 x 10^{-2} (99%)	4.46 x 10^{-5} (0%)
GW5	7.97 x 10^{-6} (2%)	4.14 x 10^{-4} (98%)	4.35 x 10^{-7} (0%)

the PDI contribution to the UR, pointing out the potential dominance of PDI over the other two SEU mechanisms.

For the ISSI SRAM, the contributions to the UR (both in absolute and percentage terms) are reported in Table VII for both the MC simulations and for the approximated Dodds' method. PDI UR for GEO quiet conditions is found to contribute for a maximum of 11% to the total UR, again pointing out that PDI effects can be considered negligible in this environment. For the other three environments, when considering the MC simulations, PDI is still the major contributor to the UR. However, it is not dominant in all the cases. At the lowest, PDI contributes to 65% for the I5 orbit and can reach 97% for the GW1 environment. The situation is quite different when considering the approximated Dodds' method. In this case, PDI never contributes less than 91% for each orbit, with a peak of 99% for GW1.

TABLE VIII

UR OF THE **CYPRESS SRAM** FROM PROTON INDIRECT AND DIRECT IONIZATION AND HIS (WITH PERCENTAGE CONTRIBUTIONS TO THE TOTAL UR IN BRACKETS) FOR EIGHT COMBINATIONS OF ORBITS AND SHIELDING CONFIGURATIONS. UR IN SEU/bit/day

Monte-Carlo			
Env.	**UR**$_{HEP}$ **(%)**	**UR**$_{LEP}$ **(%)**	**UR**$_{HI}$ **(%)**
I1	1.58 x 10^{-7} (8%)	1.88 x 10^{-6} (91%)	4.02 x 10^{-8} (1%)
I5	1.21 x 10^{-7} (21%)	4.17 x 10^{-7} (73%)	3.58 x 10^{-8} (6%)
L1	7.46 x 10^{-6} (5%)	1.37 x 10^{-4} (95%)	1.63 x 10^{-7} (0%)
L5	7.32 x 10^{-6} (23%)	2.41 x 10^{-5} (77%)	5.37 x 10^{-8} (0%)
GQ1	2.98 x 10^{-8} (11%)	1.14 x 10^{-9} (0%)	2.44 x 10^{-7} (89%)
GQ5	2.66 x 10^{-8} (12%)	2.31 x 10^{-10} (1%)	1.87 x 10^{-7} (87%)
GW1	2.70 x 10^{-4} (2%)	1.54 x 10^{-2} (96%)	3.34 x 10^{-4} (2%)
GW5	7.21 x 10^{-5} (11%)	5.48 x 10^{-4} (88%)	4.29 x 10^{-6} (1%)
Approximated Dodds' method			
Env.	**UR**$_{HEP}$ **(%)**	**UR**$_{LEP}$ **(%)**	**UR**$_{HI}$ **(%)**
I1	2.03 x 10^{-7} (6%)	3.41 x 10^{-6} (93%)	4.02 x 10^{-8} (1%)
I5	1.48 x 10^{-7} (14%)	8.65 x 10^{-7} (83%)	3.58 x 10^{-8} (3%)
L1	1.02 x 10^{-5} (4%)	2.33 x 10^{-4} (96%)	1.63 x 10^{-7} (0%)
L5	7.31 x 10^{-6} (15%)	4.20 x 10^{-5} (85%)	5.37 x 10^{-8} (0%)
GQ1	3.09 x 10^{-8} (11%)	3.54 x 10^{-9} (1%)	2.44 x 10^{-7} (88%)
GQ5	2.99 x 10^{-8} (14%)	4.10 x 10^{-9} (2%)	1.87 x 10^{-7} (84%)
GW1	1.73 x 10^{-4} (1%)	3.25 x 10^{-2} (98%)	3.34 x 10^{-4} (1%)
GW5	4.25 x 10^{-5} (4%)	1.18 x 10^{-3} (96%)	4.29 x 10^{-6} (0%)

For the Cypress SRAM, the contributions to the UR (both in absolute and percentage terms) are reported in Table VIII for both the MC simulations and for the approximated Dodds' method. In this case as well, PDI contributes to the GQ UR by 0%–2%, pointing out that PDI will not contribute to the total UR in this environment. For the other three environments, when considering MC simulations, PDI is the main contributor to the UR, it is never below 73% and it can peak at 96% for the GW1 environment. One peculiarity for the Cypress SRAM is that the HEP component of the UR is, in percentage, higher than for the other two memories. Similar to the ISSI SRAM, when considering the approximated Dodds' method, the PDI contribution to the UR becomes dominant, with an 83% lowest percentage contribution for the I5 orbit and a maximum of 98% for the GW1 environment.

The *D* factors for the RADSAGA 65-nm SRAM for both the MC and the approximated Dodds' methods are reported in Fig. 7. The plot is made to compare how the *D* factor changes with orbit, shielding, and calculation method. The RADSAGA 65-nm SRAM shows quite consistent *D* factors for almost all the orbits when calculated either using MC or with the approximated Dodds' method. Letting the GEO quiet conditions aside, regardless of the calculation method, the orbit or the shielding, the *D* factor is never below 5 and can reach up to 43 for the L1 and GW5 orbits.

The *D* factors for the ISSI SRAM for both the MC and the approximated Dodds' method are reported in Fig. 8. Note that, in this case, the data are reported in logarithmic scale to improve readability. In the case of the ISSI SRAM, the two methods may disagree by even a factor of 4 for the I5 and GW1 environments. The approximated Dodds' method predicts the highest *D* factor to be roughly 150 (for the GW1 environment). For the same orbit, the MC simulations

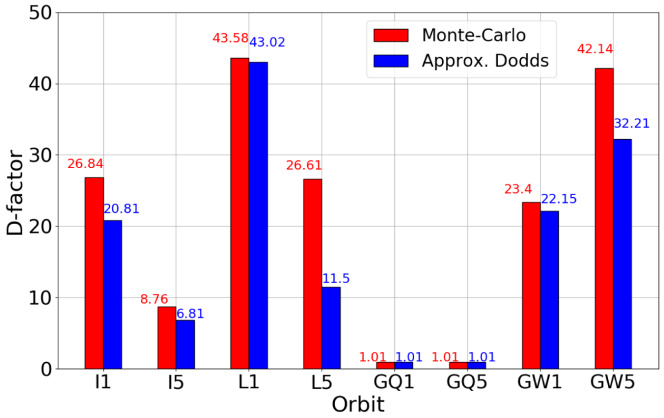

Fig. 7. *D* factors of the RADSAGA 65-nm SRAM calculated for eight combinations of orbit and shielding with the MC simulations and the approximated Dodds' method.

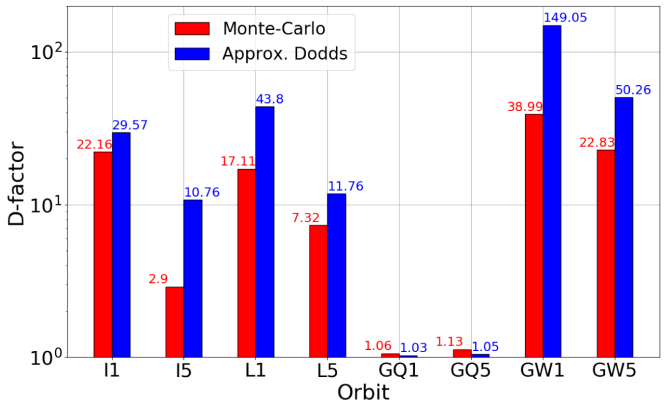

Fig. 8. *D* factors of the ISSI SRAM calculated for eight combinations of orbit and shielding with the MC simulations and the approximated Dodds' method.

predicts a factor of 39. The minimum *D* factors are found for the GQ conditions (just above 1). Letting this environment aside, the minimum would otherwise be 3 for the I5 orbit. For this same orbit, the approximated Dodds' method provides the lowest *D* factor, which is as high as 11.

The *D* factors for the Cypress SRAM for both the MC and the approximated Dodds' method are reported in Fig. 9, also in logarithmic scale. The comparison between the two methods yields similar observations as for the ISSI SRAM, though the difference, in this case, is moderate, that is, the approximated Dodds' method yields less than a factor of 2 higher *D* factors than MC for the ISS and LEO cases, with the only exception of GEO worst day. With the exception of the GQ cases, for which the *D* factor is 1 or just above, all other *D* factors are higher than 5. For MC, the highest *D* factor is 27 for the GW1 orbit and the lowest is 4 for the I5 orbit. For the approximated Dodds' method, the highest *D* factor is 65 for the GW1 orbit and the lowest is 6 for the I5 orbit.

The two methods point out quite heterogeneous contributions to the UR. In general, the MC simulations bring factors which are equal to or lower than the approximated Dodds' method. Despite representing the most optimistic prediction

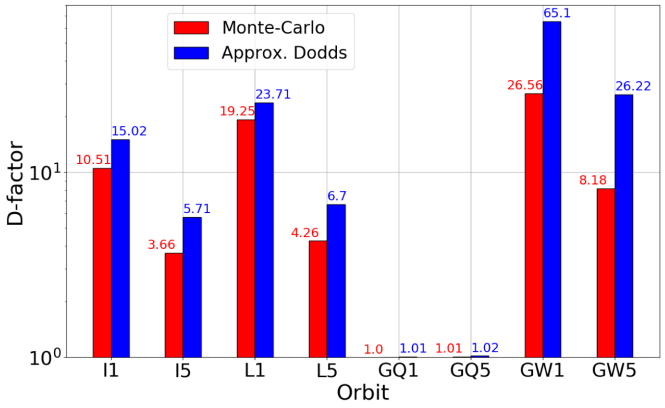

Fig. 9. *D* factors of the Cypress SRAM calculated for eight combinations of orbit and shielding with the MC simulations and the approximated Dodds' method.

case, the MC simulations still yield *D* factors that violate the safety margin of 5 established in the literature [10].

The shielding is almost always seen to provide a benefit in terms of UR in absolute value. However, it does have a quite limited impact on the *D* factors. At best, for the ISSI SRAM, the *D* factor for I5 was 7 times smaller than for I1. For the other conditions, the effect is no higher than a factor of 2. The RADSAGA 65-nm SRAM and the GEO stormy environment represent the only exception. For this case alone, the *D* factor for 500 mils is seen to be higher than for 100 mils for both methods. The reason is likely related to the wider PDI cross section peak of the RADSAGA 65-nm SRAM with respect to the other two devices, which render the RADSAGA 65-nm SRAM also more sensitive to intermediate-energy protons. Hence, 500 mils of aluminum are likely not enough to mitigate the effects of a large part of the intermediate-energy protons. In the literature [38], more realistic shielding configurations were found to yield a reduction in the PDI UR by up to a factor of 25 with respect to the spherical 100 mils aluminum shielding.

VI. *D* Factor as a Function of the Critical Charge

One advantage of the MC simulations is that they provide data over a wide range of critical charges. While losing the link to the data of these specific devices, such analysis can allow exploring how the *D* factor would vary when changing the critical charge of the model, which can be used to assess whether the device may be sensitive to direct ionization from HEPs and how the picture may change for other devices having a different critical charge. Note that the other parameters of the modeled SVs may also play a role, so this analysis will focus strictly on common observations among devices and models.

In order to use the MC data as a function of critical charge, the L1 orbit was chosen. The HI contribution to the UR was found to be negligible for this orbit. This allows neglecting the overestimated (but still negligible) low-LET HI response from MC, so that the *D* factor simplifies further

$$D(Q_{\text{crit}}) = \frac{\text{UR}_{\text{HEP}}(Q_{\text{crit}}) + \text{UR}_{\text{LEP}}(Q_{\text{crit}})}{\text{UR}_{\text{HEP}}(Q_{\text{crit}})}. \quad (2)$$

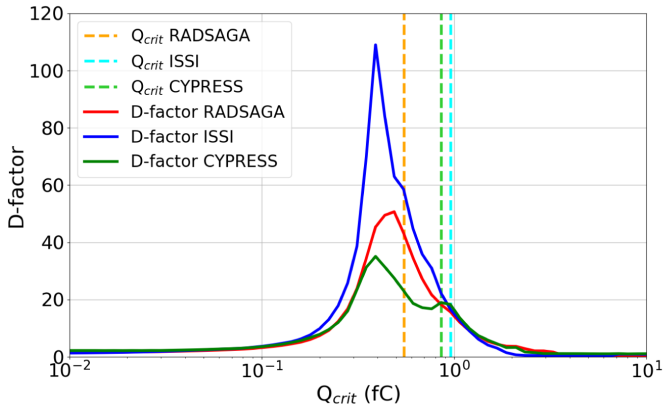

Fig. 10. *D* factors of the three devices calculated for the LEO orbit with 100 mils of aluminum shielding with the MC simulations as a function of the critical charge.

In general terms, the *D* factor will converge to 1 at high critical charge because LEPs would not deposit enough charge to trigger SEUs. At the same time, it will converge to 1 also at very low critical charge (below 0.1 fC) because such a device would also be sensitive to direct ionization from HEPs. The latter would be covered through HEP testing and would make the LEP contribution less important in relative terms.

Thus, the *D* factor is expected to reach an absolute maximum, usually at critical charges in between 0.1 and 1 fC. If the chosen critical charge is lower than that corresponding to the absolute maximum, direct ionization effects may be relevant also at energies above 20 MeV.

Fig. 10 reports the *D* factor as a function of critical charge for the three devices under consideration. For the RADSAGA 65-nm SRAM, the chosen critical charge falls very close to the peak region (which is at around 0.5 fC). This shows that this device is likely sensitive to direct ionization effects above 3 MeV and, potentially, up to 20 MeV.

For the ISSI SRAM, the chosen critical charge is just placed at the onset of the range of critical charges for which PDI becomes dominant. However, the ISSI SRAM shows an absolute maximum that can stretch up to more than 100.

The Cypress SRAM has the lowest peak in absolute value among the three devices. Another peculiarity is represented by the secondary peak located at the chosen critical charge (0.86 fC), for which the *D* factor reaches a relative maximum, which is as high as 60% of the absolute maximum at 0.4 fC. The chosen critical charge (0.86 fC) places the model almost halfway between the absolute maximum and the onset, indicating that direct ionization from HEPs is unlikely for this device.

In general, the critical charge at which the *D* factor reaches the absolute maximum is seen not to vary much among the different SV models and it occurs for a critical charge of 0.4–0.5 fC. However, the absolute value of the *D* factor may vary by far, from 35 for the Cypress SRAM to 110 for the ISSI SRAM and it seems to be strictly related to the ratio between the PDI cross section peak and the HEP saturation cross section observed experimentally.

VII. Discussion

The three devices under consideration have all proved, to different extents, to be very susceptible to direct ionization from LEPs. Experiments with mono-energetic protons exhibit ratios between the peak PDI cross sections and the high-energy saturation cross sections higher than 10^4.

When brought into an environmental context, such high and wide PDI effects were predicted to provide not only a significant contribution to the total UR, but, in most of the cases, they dominated the total UR response. Regardless of the prediction method used, the considered orbit or the shielding, PDI was found to contribute about 90% of the total UR on average, with maxima of 99%.

The corresponding *D* factors calculated for these devices in the considered environments were always on the order of a few tens, reaching maximum values above 100 for the worst case orbits. These were either low-Earth orbits for which the trapped proton fluxes are quite high or the GEO environments under the intensification of the proton fluxes provided by a strong solar activity. Shielding (varying from 100 to 500 mils of Al) was seen to have an impact, but just to a limited extent, often sufficient to reduce the *D* factor by a factor of 2.

The *D* factor is assumed to be a safety margin that one can apply to the UR calculated through Weibull fitting of the HEP and HI experimental cross sections. It is clear that safety margins make sense if they are small compared to the quantity that is margined. At least for the considered devices, this is not the case for basically any space environment (even the supposedly mild ISS environment). Considering the potential uncertainty of the UR calculation methods for PDI effects, a method based on the application of safety margins over the UR calculated from HEPs and HIs is unlikely to work. Bounding the UR with the highest *D* factor found among all the devices would mean applying always a factor of 150 to the UR calculated excluding LEPs, which will often be unrealistically pessimistic.

From the experimental data reported in other works [6], [13], it is clear that such a safety margin would provide a huge overshoot over the actual contribution of PDI to the UR of memory devices in general. More than providing a revision to the required safety margins to account for PDI when calculating the UR from HEP and HI responses, the presented data rather reinforce the need to perform experimental characterization of memory devices with either mono-energetic LEPs [31] or degraded HEP beams [6].

Some further considerations can be made on the accuracy of the proposed calculation methods. The RPP models calibrated over LEPs and HEPs proved to be very accurate for the two proton contributors, but provided some overestimation of the HI contribution with respect to the Weibull-predicted UR, which, in turn, would have reduced the *D* factor. However, for the RADSAGA 65-nm SRAM, the *D* factor would have not reduced by more than a factor of 1.5, still pointing out a quite strong PDI enhancement.

Concerning the approximated Dodds' method, it is clear that it would not exactly correspond to the experimental measurements attained by degradation of a high-energy beam.

However, this approximated method is likely not overestimating the UR by more than a factor of 5. Even when considering such a strong inaccuracy, it would still yield D factors higher than 10 for certain devices and certain orbits.

In this respect, the simplicity of the approximated Dodds' method is counterbalanced by a higher degree of inaccuracy in the UR prediction, whereas the MC simulations can be considered to provide a higher-fidelity estimation within a factor of ± 2.

As a matter of fact, it will not be possible to draw conclusion about the accuracy of current UR prediction methods for PDI unless the devices are actually tested in the space environment. Currently, the devices analyzed in this work have been considered for launch in LEO space missions. If proved to be that sensitive to the actual space radiation environment, they could be considered as a baseline to have very sensitive radiation monitors to characterize the LEP fluxes in space.

The analysis of the D factor as a function of critical charge showed that for the RADSAGA 65-nm SRAM, the worst case scenario was already reached, being the chosen critical charge so close to that of the D factor absolute maximum. This may point out an influence from direct ionization above 3 MeV, potentially extending up to 20 MeV and above. The analysis for the other two devices showed that they are still positioned at about the onset of the PDI sensitivity and still quite far from the absolute maximum.

VIII. Conclusion

Novel data and soft error prediction methods on the impact of PDI in SRAMs based on deep submicron technology and bulk Si were presented to report on the strong enhancement to the UR that would come from the observed PDI effects. The big impact seems to be related to both the relatively high peak PDI cross section, compared to the HEP saturation cross section, and to the wide energy range for which direct ionization phenomena play a role, which may extend even above 3 MeV.

Regardless of the calculation method employed, PDI contributes, on average, about 90% of the total UR. The resulting safety margins (D factors) to be applied to the UR calculated from HEP and HI experimental data generally exceed the factor of 5 previously established in the literature and can get as high as 150. Although the analyzed devices could just represent a worst case for PDI, it is suggested to pursue experimental characterization for PDI effects whenever the HI LET threshold of the device is lower than 0.4 MeV/(mg/cm^2), rather than stick to the application of a general safety margin.

Acknowledgment

The authors acknowledge Yolanda Morilla and Pedro Martìn-Holgado from CNA; Heikki Kettunen, Mikko Rossi, and Jukka Jaatinen from RADEF; Marc-Jan van Goethem, Harry Kiewiet, Emil van der Graaff, and Sytze Brandenburg from KVI; and Wojtek Hajdas, Laura Sinkunaite, and Miroslaw Marszalek from PSI for their support during data collection at the respective facilities.

Special thanks go to Helmut Puchner, from Cypress Semiconductors, for providing the information required to disable the embedded ECC within the Cypress 65-nm chip.

References

[1] K. P. Rodbell, D. F. Heidel, H. H. K. Tang, M. S. Gordon, P. Oldiges, and C. E. Murray, "Low-energy proton-induced single-event-upsets in 65 nm node, silicon-on-insulator, latches and memory cells," *IEEE Trans. Nucl. Sci.*, vol. 54, no. 6, pp. 2474–2479, Dec. 2007.

[2] D. F. Heidel *et al.*, "Low energy proton single-event-upset test results on 65 nm SOI SRAM," *IEEE Trans. Nucl. Sci.*, vol. 55, no. 6, pp. 3394–3400, Dec. 2008.

[3] M. P. King *et al.*, "Electron-induced single event upsets in static random access memories," *IEEE Trans. Nucl. Sci.*, vol. 60, no. 6, pp. 4122–4129, Dec. 2013.

[4] B. D. Sierawski *et al.*, "Muon-induced single event upsets in deep-submicron technology," *IEEE Trans. Nucl. Sci.*, vol. 57, no. 6, pp. 3273–3278, Dec. 2010.

[5] *Single Event Effects Test Method and Guidelines*, Standard ESCC 25100, European Space Components Coordination, ESA, Oct. 2014.

[6] N. A. Dodds *et al.*, "Hardness assurance for proton direct ionization-induced SEEs using a high-energy proton beam," *IEEE Trans. Nucl. Sci.*, vol. 61, no. 6, pp. 2904–2914, Dec. 2014.

[7] A. Akkerman, J. Barak, and N. M. Yitzhak, "Role of elastic scattering of protons, muons, and electrons in inducing single-event upsets," *IEEE Trans. Nucl. Sci.*, vol. 64, no. 10, pp. 2648–2660, Oct. 2017.

[8] P. Caron, C. Inguimbert, L. Artola, R. Ecoffet, and F. Bezerra, "Physical mechanisms of proton-induced single-event upset in integrated memory devices," *IEEE Trans. Nucl. Sci.*, vol. 66, no. 7, pp. 1404–1409, Jul. 2019.

[9] Z. Wu, S. Chen, J. Yu, J. Chen, P. Huang, and R. Song, "Recoil-ion-induced single event upsets in nanometer CMOS SRAM under low-energy proton radiation," *IEEE Trans. Nucl. Sci.*, vol. 64, no. 1, pp. 654–664, Jan. 2017.

[10] N. A. Dodds *et al.*, "The contribution of low-energy protons to the total on-orbit SEU rate," *IEEE Trans. Nucl. Sci.*, vol. 62, no. 6, pp. 2440–2451, Dec. 2015.

[11] B. D. Sierawski *et al.*, "Impact of low-energy proton induced upsets on test methods and rate predictions," *IEEE Trans. Nucl. Sci.*, vol. 56, no. 6, pp. 3085–3092, Dec. 2009.

[12] J. R. Schwank *et al.*, "Hardness assurance testing for proton direct ionization effects," *IEEE Trans. Nucl. Sci.*, vol. 59, no. 4, pp. 1197–1202, Aug. 2012.

[13] J. Guillermin, N. Sukhaseum, P. Pourrouquet, N. Chatry, F. Bezerra, and R. Ecoffet, "Worst-case proton contribution to the direct ionization SEU rate," in *Proc. 17th Eur. Conf. Radiat. Effects Compon. Syst. (RADECS)*, Geneva, Switzerland, Oct. 2017, pp. 330–337.

[14] R. G. Alia *et al.*, "Direct ionization impact on accelerator mixed-field soft-error rate," *IEEE Trans. Nucl. Sci.*, vol. 67, no. 1, pp. 345–352, Jan. 2020.

[15] J. Wang, J. Prinzie, A. Coronetti, and P. Leroux, "Study of the SEU sensitivity of an SRAM-Based Radiation Monitor in a 65-nm CMOS Technology," *IEEE Trans. Nucl. Sci.*, to be published.

[16] A. Coronetti *et al.*, "SEU characterization of commercial and custom-designed SRAMs based on 90 nm technology and below," in *Proc. IEEE Radiat. Effects Data Workshop Rec.*, Santa Fe, NM, USA, Nov./Dec. 2020, pp. 56–63.

[17] N. A. Dodds *et al.*, "New insights gained on mechanisms of low-energy proton-induced SEUs by minimizing energy straggle," *IEEE Trans. Nucl. Sci.*, vol. 62, no. 6, pp. 2822–2829, Dec. 2015.

[18] Y. Morilla *et al.*, "Progress of CNA to become the Spanish facility for combined irradiation testing in aerospace," in *Proc. 18th Eur. Conf. Radiat. Effects Compon. Syst. (RADECS)*, Gothenburg, Sweden, Sep. 2018, pp. 250–254.

[19] A. Virtanen, R. Harboe-Sorensen, A. Javanainen, H. Kettunen, H. Koivisto, and I. Riihimaki, "Upgrades for the RADEF facility," in *Proc. IEEE Radiat. Effects Data Workshop*, Honolulu, HI, USA, Jul. 2007, pp. 38–41.

[20] H. Kettunen *et al.*, "Low energy protons at RADEF—Application to advanced eSRAMs," in *Proc. IEEE Radiat. Effects Data Workshop (REDW)*, Paris, France, Jul. 2014, pp. 147–150.

[21] E. R. van der Graaf, R. W. Ostendorf, M.-J. van Goethem, H. H. Kiewiet, M. A. Hofstee, and S. Brandenburg, "AGORFIRM, the AGOR facility for irradiations of materials," in *Proc. Eur. Conf. Radiat. Effects Compon. Syst.*, Bruges, Belgium, Sep. 2009, pp. 451–454.

[22] W. Hajdas, F. Burri, C. Eggel, R. Harboe-Sorensen, and R. D. Marino, "Radiation effects testing facilities in PSI during implementation of the proscan project," in *Proc. IEEE Radiat. Effects Data Workshop*, Phoenix, AZ, USA, Jul. 2002, pp. 160–164.

[23] C. Weulersse, F. Miller, D. Alexandrescu, E. Schaefer, and R. Gaillard, "Assessment and comparison of the low energy proton sensitivity in 65 nm to 28 nm SRAM devices," in *Proc. 12th Eur. Conf. Radiat. Effects Compon. Syst.*, Seville, Spain, Sep. 2011, pp. 291–296.

[24] N. Seifert, B. Gill, J. A. Pellish, P. W. Marshall, and K. A. LaBel, "The susceptibility of 45 and 32 nm bulk CMOS latches to low-energy protons," *IEEE Trans. Nucl. Sci.*, vol. 58, no. 6, pp. 2711–2718, Dec. 2011.

[25] R. K. Lawrence, J. F. Ross, N. F. Haddad, R. A. Reed, and D. R. Albrecht, "Soft error sensitivities in 90 nm bulk CMOS SRAMs," in *Proc. IEEE Radiat. Effects Data Workshop*, Quebec City, QC, Canada, Jul. 2009, pp. 123–126.

[26] PSTAR. *National Institute of Standards and Technology*. Accessed: May 2020. [Online]. Available: https://physics.nist.gov/PhysRefData/Star/Text/PSTAR.html

[27] J. F. Ziegler and J. P. Biersack. *Stopping and Range of Ions in Matter*. Accessed: Aug. 2018. [Online]. Available: http://www.srim.org

[28] G. Battistoni *et al.*, "Overview of the FLUKA code," *Ann. Nucl. Energy*, vol. 82, pp. 10–18, Aug. 2015.

[29] T. T. Böhlen *et al.*, "The FLUKA code: Developments and challenges for high energy and medical applications," *Nucl. Data Sheets*, vol. 120, pp. 211–214, Jun. 2014.

[30] B. Ye *et al.*, "Low energy proton induced single event upset in 65 nm DDR and QDR commercial SRAMs," *Nucl. Instrum. Meth. Phys. Res. B, Beam Interact. Mater. At.*, vol. 406, pp. 443–448, Sep. 2017.

[31] J. A. Pellish *et al.*, "Criticality of low-energy protons in single-event effects testing of highly-scaled technologies," *IEEE Trans. Nucl. Sci.*, vol. 61, no. 6, pp. 2896–2903, Dec. 2014.

[32] J. M. Trippe *et al.*, "Predicting muon-induced SEU rates for a 28-nm SRAM using protons and heavy ions to calibrate the sensitive volume model," *IEEE Trans. Nucl. Sci.*, vol. 65, no. 2, pp. 712–718, Feb. 2018.

[33] R. A. Reed *et al.*, "Impact of ion energy and species on single event effects analysis," *IEEE Trans. Nucl. Sci.*, vol. 54, no. 6, pp. 2312–2321, Dec. 2007.

[34] CREME. *Vanderbilt University*. Accesses: May 2020. [Online]. Available: https://creme.isde.vanderbilt.edu

[35] E. L. Petersen, J. C. Pickel, J. H. Adams, and E. C. Smith, "Rate prediciton for single event effects," *IEEE Trans. Nucl. Sci.*, vol. 39, no. 6, pp. 1577–1599, Dec. 1992.

[36] E. H. Cannon *et al.*, "Heavy ion, high-energy, and low-energy proton SEE sensitivity of 90-nm RHBD SRAMs," *IEEE Trans. Nucl. Sci.*, vol. 57, no. 6, pp. 3493–3499, Dec. 2010.

[37] L. D. Edmonds and K. J. Edmonds, "A method for estimating SEU rates from protons by direct ionization," *IEEE Trans. Nucl. Sci.*, vol. 55, no. 5, pp. 2666–2678, Oct. 2008.

[38] J. A. Pellish *et al.*, "Impact of spacecraft shielding on direct ionization soft error rates for sub-130 nm technologies," *IEEE Trans. Nucl. Sci.*, vol. 57, no. 6, pp. 3183–3189, Dec. 2010.